Les Cahiers du GERAD ISSN: 0711–2440

Spatio-temporal flexibility requirement envelopes for low-carbon power system energy management

Y. Huo, F. Bouffard, G. Joós

G–2019–35

May 2019

GERAD HEC Montréal
3000, chemin de la Côte-Sainte-Catherine
Montréal (Québec) Canada H3T 2A7

Tél. : 514 340-6053
Téléc. : 514 340-5665
info@gerad.ca
www.gerad.ca

Spatio-temporal flexibility requirement envelopes for low-carbon power system energy management

Yuchong Huo [a,b]

François Bouffard [a,b]

Géza Joós, [b]

[a] *GERAD, Montréal (Québec), Canada, H3T 2A7*

[b] *Department of Electrical and Computer Engineering, McGill University, Montréal (Québec) Canada, H3A 0E9*

yuchong.huo@mail.mcgill.ca
francois.bouffard@mcgill.ca
geza.joos@mcgill.ca

May 2019
Les Cahiers du GERAD
G–2019–35

Abstract: The deepening penetration of renewable power generation is challenging how the minute balancing of supply and demand is carried out by power system operators. Several proposals to short-term operational planning rely on robust optimization to offer guarantees on the ability of the operator to meet a wide array of possible scenarios. The main downside of these approaches is their conservative results whose operating costs and/or carbon tally may be sub-economical. Such results come by because these approaches put emphasis often on very low-probability portions of the uncertainty set they consider. Moreover, these approaches also often ignore the inherent time and spatial couplings of wind and solar generation variability. In this paper, we seek to reduce the conservativeness of these uncertainty sets by proposing the concept of spatio-temporal flexibility requirement envelopes. We show how it is able to efficiently capture and model the temporal trends and spatial correlation of multisite renewable generation and load. A mathematical program for energy scheduling is also developed using the projections of this envelope. We showcase the use and advantages of spatio-temporal flexibility requirement envelopes and their associated scheduling approach in a microgrid and on a modified IEEE Reliability Test System.

Keywords: Energy management, flexibility, power system operation, renewable power generation, spatio-temporal correlation

Résumé : L'accroissement de la proportion d'énergies renouvelables fluctuantes représente un défi important pour les exploitants de réseaux électriques. Il existe plusieurs méthodes fondées sur l'optimisation robuste dont le but est de faire l'ordonnancement à court- terme de la production afin d'offrir aux exploitants un bon niveau de certitude en lien avec leurs objectifs de bonne conduite des réseaux et les niveaux de fluctuation de la production renouvelable. Le principal désavantage de ces méthodes est son niveau de conservatisme pouvant mener à des hausses de coûts d'exploitation et des bilans carbone des réseaux. Ces résultats découlent de l'accent que ses méthodes donnent aux portions très peu probables des ensembles d'incertitudes qu'ils considèrent. De plus, ces méthodes ignorent généralement le fait que le niveau de variabilité de la production solaire et éolienne varie dans le temps et que celle-ci est également corrélée spatialement. Dans cet article, nous proposons de réduire le niveau de conservatisme de ces ensembles d'incertitude en développant le concept des enveloppes d'exigences de flexibilité spatio-temporelles. Nous démontrons comment ces enveloppes sont en mesure de représenter fidèlement les tendances temporelles et les corrélations entre différents sites de production d'énergie renouvelable en plus de celle de la demande. Un modèle de programmation mathématique est également développé pour effectuer l'ordonnancement des ressources via la projection des enveloppes d'exigences de flexibilité. Nous illustrons le fonctionnement et les avantages de notre proposition dans le cadre d'un microréseau et d'un réseau de transport d'électricité (IEEE Reliability Test System).

Mots clés : Gestion de l'énergie, flexibilité, fonctionnement d'un système énergétique, production d'énergie renouvelable, corrélation spatio-temporelle

Acknowledgments: This work was supported in part by the Natural Sciences and Engineering Research Council of Canada, Ottawa (Ontario) and InnovÉÉ, Montreal (Québec).

Nomenclature

The main symbols used in the paper are defined here. Further symbols will be defined as required.

Sets	
Ξ_i	Set of conventional generators.
Ξ_m	Set of storage assets.
Ξ_n	Set of buses.
Ξ_H	Set of intra-hourly receding-horizon time.
Ξ_q	Set of movement directions in a flexibility requirement envelope.
Indices	
i	Index of conventional generators.
m	Index of storage assets.
n	Index of buses.
q	Index of movement directions in a flexibility requirement envelope (up: $\uparrow$, down: $\downarrow$).
t	Actual operating time.
τ	Index of intra-hourly receding-horizon time.
Variables	
$x_i^c(\tau, q)$	Envelope tracking variable of the power output of generator i at time τ.
$u_i^c(\tau, q)$	Commitment status (binary) of generator i at time τ.
$x_m^{o\pm}(\tau, q)$	Positive (+) and negative (−) parts of envelope tracking variable of the power output of storage m at time τ.
$u_m^{o\pm}(\tau, q)$	Commitment status (binary) of charging (+)/discharging (−) of storage m at time τ.
$s_m^o(\tau, q)$	Envelope tracking variable of energy hold of storage m at time τ.
$x_n^d(\tau, q)$	Envelope tracking variable of load curtailment at bus n at time τ.
$x_n^w(\tau, q)$	Envelope tracking variable of wind power curtailment at bus n at time τ.
$x_n^s(\tau, q)$	Envelope tracking variable of solar power curtailment at bus n at time τ.
$g_i^c(t)$	Power output of generator i at time t.
$g_m^o(t)$	Power output of storage m at time t.
$s_m^o(t)$	Energy hold of storage m at time t.
Parameters	
$d_n(t)$	Load at bus n at time t.
$\delta_n^w(t)$	Output of wind farm at bus n at time t.
$\delta_n^s(t)$	Output of solar farm at bus n at time t.
$e_A^q(\tau)$	System-wide flexibility requirement envelope at time τ.
$e_{Fl}^q(\tau)$	Flexibility requirement envelope applying to transmission line l at time τ.

1 Introduction

The main challenge of integrating renewable generation into a power system is the management of the increased disturbances in power balancing. These disturbances are caused by the inherent variability and uncertainty of renewable generation. Traditional power system operation paradigms are becoming less capable of handling this challenge, which leads to the study of the emerging concept of power system flexibility [1, 2]. Flexibility is the ability of a system to react to disturbances sufficiently fast in order to keep the system secure [3]. Thus, a power system should have sufficient flexibility to cope with increasing levels of renewable generation so that economic and secure operation can be maintained.

Previous studies used stochastic methods for scheduling flexibility in the form of ancillary services (reserves, especially) [4], [5]. Stochastic methods are effective in reducing operating costs. However, they do suffer from computational burdens caused by exponentially increasing scenarios [6], [7]. Recently, robust optimization has been used extensively in operational planning of flexibility mainly for its tractable computational cost and its ability to provide certainty to operators. This approach uses an uncertainty set to describe the flexibility requirement of a power system [8]. Usually, this uncertainty set considers worst-case realizations of uncertain renewable generation and load. Many different modeling approaches for uncertainty sets have been proposed in last few years. References [2], [9] proposed the concept of the flexibility requirement envelopes to capture the intra-hourly flexibility needs entailed by variable renewable generation. A polytope based approach was developed in [3] for constructing uncertainty sets in the presence of transmission limits in a multi-area power system.

In [10], [11], ellipsoidal uncertainty sets are used to model geographically distributed renewable energy sources.

Although robust optimization approaches secure the system according to very stringent reserve requirements, it is easy to have sub-economical results due to considerations of extreme potential events [12]. Intensive research activity is investigating solutions to alleviate this problem. It is suggested in [11] that considering statistical characteristics such as spatial correlation and diurnal or seasonal trends of renewable generation can effectively reduce the conservativeness and improve the accuracy of uncertainty sets. This is because such information is very helpful in eliminating unlikely-to-happen scenarios. It is in this spirit that in this paper we propose a modeling technique for uncertainty sets which we call *spatio-temporal flexibility requirement envelopes* as a natural extension of the original proposal of [2]. It seeks to reduce the conservativeness of uncertainty sets by representing the temporal trends and the spatial correlation of multisite renewable generation and load demand. We propose a framework for applying this envelope to power system energy management.

Compared to previous work, our proposed method has the following features: First, it extends the notion of flexibility requirement envelopes proposed in [2] and [9] by comprehensively capturing the trends and correlation of multiple site renewable generation and loads in power system. Other existing works such as [3] and [7] overlook these statistical properties, while [10] only considers spatial correlation. Second, this approach can be applied in security-constrained unit commitment and dynamic dispatch problems, capturing the effects of space-correlated renewable generation assets on the network and its constraints.

The remainder of this paper is organized as follows. The modeling methodology of spatio-temporal flexibility requirement envelopes is presented in Section II. Next, we introduce how to use spatio-temporal envelopes in power system energy management problems in Section III. Section IV conducts two case studies to show the effectiveness of our proposed approach, before concluding in Section V.

2 Modeling of spatio-temporal flexibility requirement envelope

2.1 Methodology

This section introduces the procedure for building a spatio-temporal flexibility requirement envelope. The inputs of the process are historic (or possibly synthetic) wind speed time series, solar power time series and uncertain load demand time series.

Step 1 Detrending: For a solar power time series $\delta_n^s(t)$ at bus n in day time, we compute $\delta_n^{s\prime}(t)$, the detrended solar power time series [13]:

$$\delta_n^{s\prime}(t) = \frac{\delta_n^s(t)}{\delta_n^{CS}(t)} \tag{1}$$

where $\delta_n^{CS}(t)$ is the output of solar power under the clear-sky irradiance (theoretical maximum of solar power caused by the periodical movements of the earth and the sun) at bus n at time t.

Similarly, we calculate $\omega_n'(t)$, the detrended wind speed or uncertain load demand time series at bus n [14]:

$$\omega_n'(t) = \frac{\omega_n(t) - \mu_n^M(t)}{\sigma_n^M(t)} \tag{2}$$

where $\omega_n(t)$ is the original time series, and $\mu_n^M(t)$ and $\sigma_n^M(t)$ are its estimated mean and standard deviation calculated following the method used in [15]:

$$\mu_n^M(t) = \frac{1}{M}\sum_{k=0}^{M-1}\omega_n(t-k) \tag{3}$$

$$\sigma_n^M(t) = \sqrt{\frac{1}{M-1}\sum_{k=0}^{M-1}\left(\omega_n(t-k) - \mu_n^M(t)\right)^2} \tag{4}$$

where M is the length of the time window for calculating $\mu_n^M(t)$ and $\sigma_n^M(t)$.

Step 2 Principal component analysis: In this step, $\omega_n'(t)$ and $\delta_n^{s\prime}(t)$ are transformed into Gaussian time series onto which principal component analysis (PCA) is performed. The goal here is to decompose the factors driving the variability processes into independent variability components. The details of the transformation are provided in Appendix A.

Step 3 Principal component-wise flexibility requirement envelope construction: For each principal component (PC), we build a flexibility requirement envelope $\{e_j^{\downarrow}, e_j^{\uparrow}\}$ using the method presented in [2]. Here $\{e_j^{\downarrow}, e_j^{\uparrow}\}$ is the flexibility requirement envelope for the jth $(1 \leq j \leq J)$ PC.

Step 4 Envelope construction in the PC domain: Construct a J-dimensional hypercube $\mathbf{E}'(\tau)$ for all the lookahead times $\tau \in \Xi_H$ using the flexibility requirement envelope of all J PC generated in Step 3. Because the PC are independent from each other, we use the Cartesian product:

$$\begin{aligned}\mathbf{E}'(\tau) = \{e_1^{\uparrow}(\tau), e_1^{\downarrow}(\tau)\} \times \{e_2^{\uparrow}(\tau), e_2^{\downarrow}(\tau)\} \times \cdots \\ \times \{e_{J-1}^{\uparrow}(\tau), e_{J-1}^{\downarrow}(\tau)\} \times \{e_J^{\uparrow}(\tau), e_J^{\downarrow}(\tau)\}\end{aligned} \tag{5}$$

Step 5 Mapping of PC envelope onto actual quantities' domain: Construct the hypercube $\mathbf{E}(\tau)$ by inverting the PCA transform using (30), following by its mapping back to the time domain reverting (28).

Step 6 Re-trending: Re-insert the trends eliminated previously in (1) and (2).

Step 7 Wind power curve: Transform the wind speed envelope into its corresponding wind power generation. In this paper we follow the method in [11] and [14]. The aggregate power curve for each wind farm is used moving forward; this curve can be estimated using observed wind power-wind speed pairs from wind farms.

2.2 Discussion

The output of the procedure described above is a multidimensional envelope $\mathbf{E}(\tau)$. It encompasses the vast majority of possible realizations of wind power, solar power, and uncertain load looking ahead τ units of time later, as seen from the current time. Connecting the elements of $\mathbf{E}(\tau)$ at all τ results in the spatio-temporal flexibility requirement envelope $\mathbf{E}$.

Step 1 extracts and removes the temporal trends of the input time series. The temporal trends are removed because the application of PCA in Step 2 requires that the input time series are stationary. With (2), wind power and load demand may display diurnal and seasonal trends. As a result, M should be selected based on the features of the trends of the data. The removed trends are re-incorporated in Step 6.

Step 1 captures the spatial correlation of all the input time series. The spatial dependency is removed in Step 2, and the resulting PC are independent of each other. Thus, there is no need to consider the impact of other PC when we build flexibility requirement envelopes for each PC in Step 3, and when we combine them in Step 4; this is a feature which greatly simplifies the process. The spatial dependency structure is re-inserted in Step 5 by mapping $\mathbf{E}'$ onto $\mathbf{E}$. This guarantees that the spatio-temporal flexibility requirement envelope $\mathbf{E}$ captures the spatial correlation between all the original time series.

3 Spatio-temporal flexibility requirement envelopes in power system energy management

3.1 Projection

When carrying out power system scheduling and dispatch, we are interested in quantifying the impact of the uncertainties of renewable generation and loads on the system net load (i.e., load less renewable generation output) and on the flows in transmission lines. This information is necessary to pre-position dispatchable units in power system to guarantee secure and economic operation. In this section, we show that the impact of uncertainties on the net load and transmission line flows can be quantified by projecting spatio-temporal flexibility requirement envelopes. This idea is illustrated in Figure 1 in the case of a two-dimensional envelope.

In Figure 1(a), y_{n_1} and y_{n_2} represent the power outputs of two uncertainty sources located at bus n_1 and n_2. They could be wind power, solar power or uncertain load. The vast majority of their plausible realizations after τ units of time are bounded in the envelope $\mathbf{E}(\tau)$. From Figure 1(a), we find that the maximum and minimum values of $y_{n_1} + y_{n_2}$ can be obtained by maximizing and minimizing the projection of $\mathbf{E}(\tau)$ onto the vertical axis along the direction of $y_{n_1} + y_{n_2}$. If we connect the maximum and the minimum values of the projection at all τ, we can get a flexibility requirement envelope which encompasses the vast majority (e.g., $\pm 3\sigma$) of possible realizations of $y_{n_1} + y_{n_2}$ for $\tau \in \Xi_H$.

At the same time, the impact of y_{n_1} and y_{n_2} on the power flow in transmission line l is found by calculating $h_{ln_1} y_{n_1} + h_{ln_2} y_{n_2}$ whose maximum/minimum values can also be quantified by projection (along the direction of $h_{ln_1} y_{n_1} + h_{ln_2} y_{n_2}$), as is shown in Figure 1(b)). Here, h_{ln_1} and h_{ln_2} are Power Transfer Distribution Factors (PTDF) describing the sensitivities of power flow on line l to the changes of active power injection at bus n_1 and n_2. Again, by connecting the maximum and the minimum values of the projection at all τ, we can get a flexibility requirement envelope that encompasses the vast majority of possible realizations of $h_{ln_1} y_{n_1} + h_{ln_2} y_{n_2}$ for $\tau \in \Xi_H$.

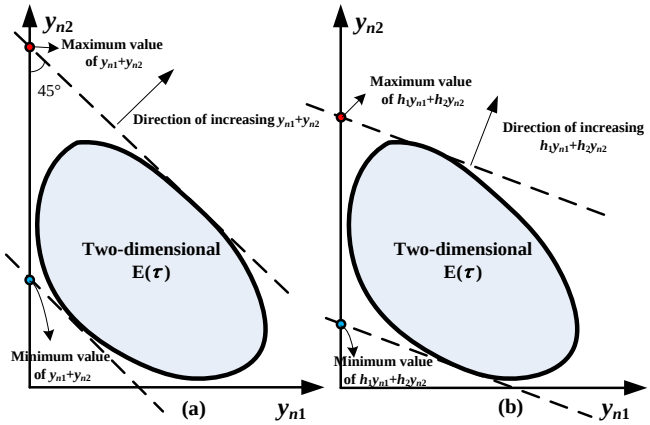

Figure 1: Projection of spatio-temporal flexibility requirement envelope.

In general, we obtain projections for flexibility requirement envelopes moving forward in $\tau \in \Xi_H$ by solving

$$\begin{aligned} e_A^{\uparrow}(\tau) &= \max_{\mathbf{Y} \in \mathbf{E}(\tau)} (\mathbf{1} \cdot \mathbf{Y}), \qquad e_A^{\downarrow}(\tau) = \min_{\mathbf{Y} \in \mathbf{E}(\tau)} (\mathbf{1} \cdot \mathbf{Y}) \\ e_{F_l}^{\uparrow}(\tau) &= \max_{\mathbf{Y} \in \mathbf{E}(\tau)} (\mathbf{H}_l \cdot \mathbf{Y}), \quad e_{F_l}^{\downarrow}(\tau) = \min_{\mathbf{Y} \in \mathbf{E}(\tau)} (\mathbf{H}_l \cdot \mathbf{Y}) \end{aligned} \tag{6}$$

Here, $\mathbf{Y}$ is the column vector consisting of active power injections from the uncertainty sources (including wind power, solar power and uncertain loads) at each bus. The vector $\mathbf{1}$ is a row vector of ones of the same length as $\mathbf{Y}$. The row vector $\mathbf{H}_l$ consists of PTDFs that describe the change of the power flow in line l with respect to the active power injection at each bus. Hence, $\{e_A^{\uparrow}, e_A^{\downarrow}\}$ is the flexibility requirement envelope for the aggregate output of all uncertainty sources, while $\{e_{F_l}^{\uparrow}, e_{F_l}^{\downarrow}\}$ is the flexibility

requirement envelope associated with transmission line l. Moreover, at the current time t where $\tau = 0$, the envelopes collapse to the current operating points: $e_A^{\uparrow}(0) = e_A^{\downarrow}(0) = \sum_n \left(d_n(t) - \delta_n^w(t) - \delta_n^s(t)\right)$ and $e_{F_l}^{\uparrow}(0) = e_{F_l}^{\downarrow}(0) = \sum_n h_{ln}\left(d_n(t) - \delta_n^w(t) - \delta_n^s(t)\right)$.

3.2 Short-term power system planning using spatio-temporal flexibility requirement envelopes

The following mathematical program is developed for receding-horizon power system energy scheduling and dispatching where spatio-temporal flexibility requirement envelopes are used to drive the current and forward-looking decisions.

1) Objective: The objective (7) is to minimize the cost of dispatchable generation ($c_i(\cdot)$) at the current time t ($\tau = 0$), while considering the forward-looking horizon $t + \tau$ for $\Xi_H = \{0, 1, 2, \cdots, T_H\}$, where T_H is the length of horizon. We perform this minimization also considering the flexibility requirement envelope directions, $\Xi_q = \{\uparrow, \downarrow\}$, penalties for load and renewable generation curtailment π^d and π^δ and a discounting factor $\gamma(\tau) \leq 1$ which weighs the forward-looking steps against the current-time costs.

$$\min \sum_{\tau \in \Xi_H, q \in \Xi_q} \gamma(\tau) \left[\sum_{i \in \Xi_i} c_i(x_i^c(\tau, q), u_i^c(\tau, q)) + \sum_{n \in \Xi_n} \left(\pi^d x_n^d(\tau, q) + \pi^\delta x_n^w(\tau, q) + \pi^\delta x_n^s(\tau, q) \right) \right] \tag{7}$$

2) Power balance for up-going and down-going envelopes $q \in \Xi_q$ and all forward-looking times $\tau \in \Xi_H$:

$$e_A^q(\tau) - \sum_{i \in \Xi_i} x_i^c(\tau, q) - \sum_{m \in \Xi_m} \left(x_m^{o+}(\tau, q) - x_m^{o-}(\tau, q) \right) + \sum_{n \in \Xi_n} \left(x_n^w(\tau, q) + x_n^s(\tau, q) - x_n^d(\tau, q) \right) = 0 \tag{8}$$

3) Transmission capacity constraints of line l for up-going and down-going envelopes $q \in \Xi_q$ and all forward-looking times $\tau \in \Xi_H$:

$$-f_l^{\max} - e_{F_l}^q(\tau) \leq f_l(\tau, q) \leq f_l^{\max} - e_{F_l}^q(\tau) \tag{9}$$

where

$$\begin{aligned} f_l(\tau, q) = \sum_{n \in \Xi_n} h_{ln} \Big[& \sum_{i \in \mathcal{N}(n)} x_i^c(\tau, q) \\ & + \sum_{m \in \mathcal{N}(n)} \left(x_m^{o+}(\tau, q) - x_m^{o-}(\tau, q) \right) \\ & + x_n^d(\tau, q) - x_n^w(\tau, q) - x_n^s(\tau, q) \Big] \end{aligned} \tag{10}$$

and $f_l^{\max}$ is the maximum allowed power flow in line l. The summations over $\mathcal{N}(n)$ are used to map the locations of generators and storage assets onto nodes of the network.

4) Bounds on load and renewable generation curtailment at bus $n \in \Xi_n$ for $q \in \Xi_q$ and $\tau \in \Xi_H$:

$$0 \leq x_n^d(\tau, q) \leq d_n(t) \tag{11}$$

$$0 \leq x_n^w(\tau, q) \leq \delta_n^w(t) \tag{12}$$

$$0 \leq x_n^s(\tau, q) \leq \delta_n^s(t) \tag{13}$$

5) Consistency of dispatch decisions and envelope tracking at current time t ($\tau = 0$): We note that at the current time t, by necessity, we require

$$g_i^c(t) = x_i^c(0, \uparrow) = x_i^c(0, \downarrow) \tag{14}$$

$$\begin{aligned} g_m^o(t) &= x_m^{o+}(0, \uparrow) - x_m^{o-}(0, \uparrow) \\ &= x_m^{o+}(0, \downarrow) - x_m^{o-}(0, \downarrow) \end{aligned} \tag{15}$$

$$s_m^o(t) = s_m^o(0, \uparrow) = s_m^o(0, \downarrow) \tag{16}$$

6) Capacity and ramp constraints on dispatchable generation $i \in \Xi_i$ for $q \in \Xi_q$ and $\tau \in \Xi_H$:

$$u_i^c(\tau,q) g_i^{c\,\min} \leq x_i^c(\tau,q) \leq u_i^c(\tau,q) g_i^{c\,\max} \tag{17}$$

$$x_i^c(\tau-1,q) - x_i^c(\tau,q) \leq r_i^{\text{cdn}} u_i^c(\tau,q) + r_i^{\text{csd}}(u_i^c(\tau-1,q) - u_i^c(\tau,q)) + g_i^{c\,\max}(1 - u_i^c(\tau-1,q)) \tag{18}$$

$$x_i^c(\tau,q) - x_i^c(\tau-1,q) \leq r_i^{\text{cup}} u_i^c(\tau-1,q) + r_i^{\text{csu}}(u_i^c(\tau,q) - u_i^c(\tau-1,q)) + g_i^{c\,\max}(1 - u_i^c(\tau,q)) \tag{19}$$

where $g_i^{c\,\max}$ and $g_i^{c\,\min}$ are the maximum and minimum power limit of generator i. Upward and downward ramping limits are r_i^{cup} and r_i^{cdn}, respectively, and r_i^{csu} and r_i^{csd} are start-up and shut-down ramping limits.

7) Capacity and energy constraints on storage $m \in \Xi_m$ for $q \in \Xi_q$ and $\tau \in \Xi_H$:

$$0 \leq x_m^{o+}(\tau,q) \leq u_m^{o+}(\tau,q) g_m^{o\,\max} \tag{20}$$

$$0 \leq x_m^{o-}(\tau,q) \leq u_m^{o-}(\tau,q) g_m^{o\,\min} \tag{21}$$

$$s_m^{o\,\min} \leq s_m^o(\tau,q) \leq s_m^{o\,\max} \tag{22}$$

$$s_m^o(\tau,q) = s_m^o(\tau-1,q) - x_m^{o+}(\tau,q) T_\Delta (\eta_m^d)^{-1} + x_m^{o-}(\tau,q) T_\Delta \eta_m^c \tag{23}$$

$$u_m^+(\tau,q) + u_m^-(\tau,q) = 1 \tag{24}$$

where $g_m^{o\,\max}$ and $g_m^{o\,\min}$ are the maximum and minimum power limit of storage asset m. The maximum and minimum energy limits are $s_m^{o\,\max}$ and $s_m^{o\,\min}$, respectively, η_m^c and η_m^d are the charging and discharging efficiencies, and T_Δ is the actual time duration between two time steps.

4 Case studies

In this section, we illustrate the joint application of the flexibility requirement envelope computation approach along with its application to generation scheduling in two specific contexts.

4.1 Microgrid

This first case study showcases our proposed approach in a simple grid-connected microgrid, whose single-line diagram is shown in Figure 2. This microgrid includes a critical load, a curtailable load, a solar farm, a diesel generator and storage.

The parameters of diesel generator and storage are provided in Appendix B. The minimum and maximum values of curtailable load are 50 kW and 350 kW. The critical load is constant at 50 kW. The maximum power output of solar farm is 150 kW. The length of each lookahead time step is $T_\Delta = 5$ min, and the length of the receding horizon $T_H = 12$ (for a total lookahead time of 60 minutes) at every scheduling time t. The power exchange requirement at the point of common coupling (PCC) is kept constant for each day of the year. We set this requirement to be the minimal net load of any given day. Uncertainties come from solar generation and curtailable load, for which we consider a full year worth of data records.

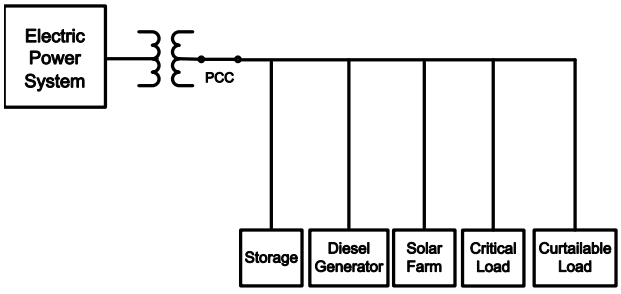

Figure 2: Diagram of microgrid under study.

The curtailable load data comes from a village in the Canadian province of Quebec, and the solar power data is taken from [16]; the time series are geographically independent from each other. Thus, in this case study we only focus on the temporal trends of solar power and curtailable load. Also, network constraints are ignored here. While we assume that $\gamma(\tau) = 1$ for all τ, three energy scheduling policies are calculated for comparison purposes:

Strategy 1: This is the proposed flexibility-based energy scheduling strategy using (7)–(24). The spatio-temporal flexibility requirement envelope is generated using the steps presented in Section 2. The length of time window M is set to be one hour.

Strategy 2: This is also a flexibility-based strategy. However, we neglect the temporal trends of curtailable load and solar power. We still use (7)–(24) to perform energy scheduling. Steps 1 and 6 are skipped when generating spatio-temporal flexibility requirement envelope.

Strategy 3: This is a myopic strategy. We set the length of the receding horizon T_H to zero, such that there is no energy management looking forward.

Figure 3 shows the evolution of curtailable load and solar generation in January. The average value of curtailable load changes almost everyday. Also, solar generation shows a clear diurnal trend. Figure 4 shows the flexibility requirement envelope for the net load generated for Strategies 1 and 2 on two different days and times. We observe that the envelopes generated by Strategy 2 are identical. This is because Strategy 2 ignores the temporal trends of curtailable load and solar power. However, the envelopes generated by Strategy 1 on January 1st are much less conservative than those of Strategy 2, while on January 6th they have similar conservativeness. The reason behind this observation can be found in Figure 3. The curtailable load is more fluctuating on January 6th than on January 1st. Strategy 1 captures this feature and adjusts the conservativeness of the envelope.

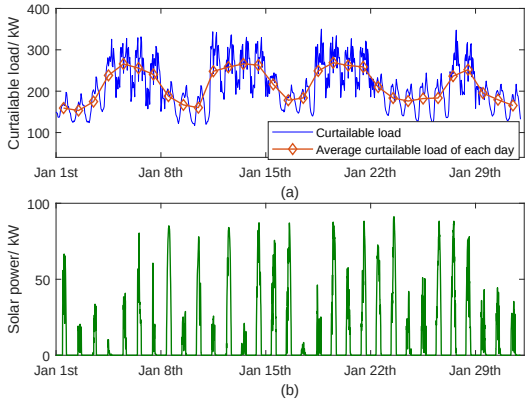

Figure 3: Power profile of (a) curtailable load and (b) solar generation in January.

Though the flexibility requirement envelope generated by Strategy 1 is sometimes less conservative, it can be found that the net load trajectory always stays inside its envelope. Figure 5 studies the flexibility requirement envelope for solar power at different times on January 1st. This envelope can be generated by projecting the spatio-temporal flexibility requirement envelope onto the solar power axis. It can be observed that the envelopes generated by Strategy 1 adjust their shapes according to the theoretical maximum of solar power (solar power under clear-sky irradiance), which is changing all the time. However, the envelopes generated by Strategy 2 cannot capture this feature, and its envelopes go beyond the theoretical maximum at 11:20 and 17:10, which should be impossible for solar power.

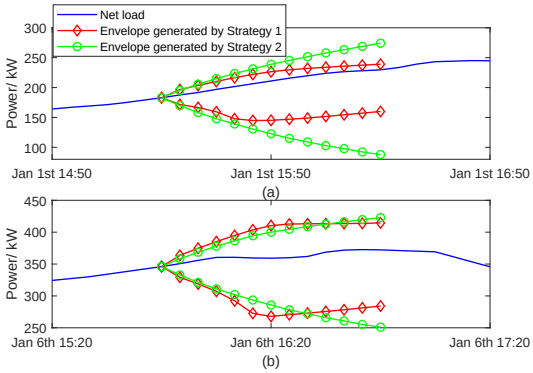

Figure 4: Flexibility requirement envelope for net load generated by Strategies 1 and 2.

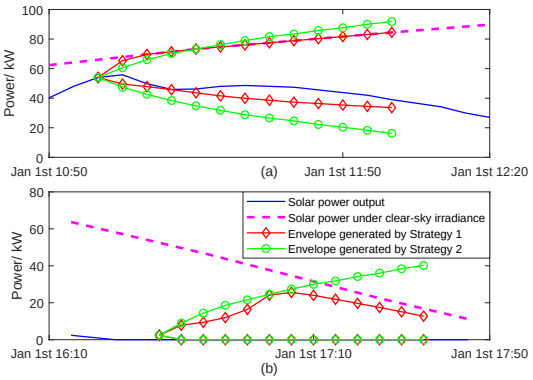

Figure 5: Flexibility requirement envelope for solar power generated by Strategies 1 and 2.

Next we look into the performance of three strategies in carrying out energy dispatching for the microgrid. We calculate three performance metrics. They are total generation cost (TGC)—where we assume quadratically-varying costs—, energy not served (ENS) and energy curtailed (EC)

$$\text{TGC} = \sum_{t} \sum_{i \in \Xi_c} \left(a_i g_i^c(t)^2 + b_i g_i^c(t) + c_i u_i^c(t) \right) \tag{25}$$

$$\text{ENS} = T_\Delta \sum_{t} \sum_{n \in \Xi_n} x_n^d(t) \tag{26}$$

$$\text{EC} = T_\Delta \sum_{t} \sum_{n \in \Xi_n} (x_n^w(t) + x_n^s(t)) \tag{27}$$

Table 1 displays the performance of each energy scheduling strategy for an entire year of operation. The percentage changes of cost are taken with respect to the myopic strategy (Strategy 3). All strategies have a good performance in terms of ENS and EC, but there are significant cost differences across strategies. A daily evolution of the energy scheduling results on January 1st under Strategies 1–3 can be seen in Figure 6. Figure 7 shows the storage's energy holding under the three strategies on January 1st. It can be observed that the diesel generator always charges storage when it is turned on under Strategies 1 and 2. When the storage energy holding is high and the remaining net load cannot be covered by the PCC, the storage is dispatched to serve the remaining net load, and Strategy 1 and Strategy 2 will turn off the diesel generator and let the storage work alone. This leads to significant decrease in total generation cost.

We can also find that the diesel generator seldom charges the storage under the myopic strategy. Thus, when the stored energy in the storage is used up, the energy holding of the storage asset stays at its lower bound unless there is excess power in the system again (e.g., when the output of diesel generator stays at its minimum limit). Remembering that the envelopes for net load on January 1st

are much more conservative under Strategy 2 as seen in Figure 4, the storage energy holding under Strategy 2 is always lower than that of Strategy 1. Thus, the flexibility of the storage is not exploited as well by Strategy 2 in comparison to Strategy 1, which contributes to drive the cost higher.

Table 1: Microgrid dispatching strategies' performance.

Scheduling policy	Performance metrics		
	TGC (k$)	ENS (kWh)	EC (kWh)
Strategy 1	304.6 (−29.4%)	0.03	0
Strategy 2	327.8 (−24.0%)	0.03	0
Strategy 3 (bench)	431.3	22.8	0

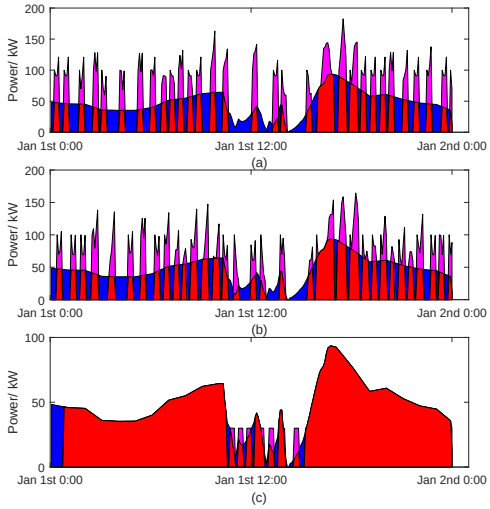

Figure 6: Daily evolution of the energy scheduling results under (a) Strategy 1, (b) Strategy 2 and (c) Strategy 3. Blue areas indicate load supply by storage, and red areas indicate load supply by the diesel generator. Magenta areas indicate diesel generator use to charge the storage asset.

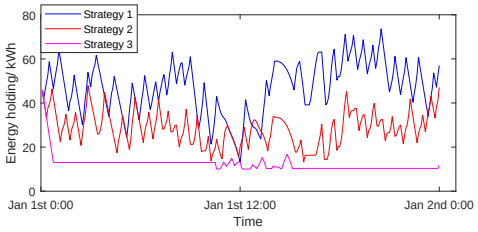

Figure 7: Daily evolution of energy holding in storage under Strategies 1–3.

Finally, Figure 8 shows how the total generation cost varies with the length of time window M when we detrend the time series of curtailable load in Strategy 1. We observe that initially the total generation cost has a sharp decline, indicating the intrinsic value of the lookahead time up until M is equal to one hour. The subsequent increase in TGC as M grows is indicative of the fact in the longer term the character of variability tends to change. The second local minimum at 16 hours reflects the periodicity of load and solar power over a 24 hour cycle.

4.2 Transmission system

Next, we illustrate our proposed approach is tested on a modified IEEE Reliability Test System (RTS). The data of the network and the load profile, generating unit ramp rates, minimum and maximum power outputs, minimum up and down times are all found in [17]. For convenience, start-up and shut-down ramps of a unit are set to be its minimum and maximum power output, respectively. We

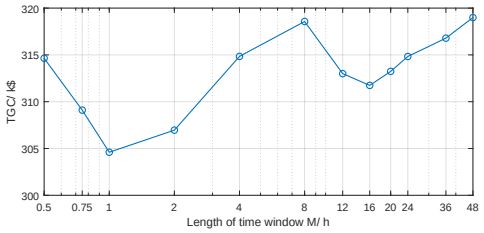

Figure 8: Effect of the length of time window M on the total generation cost in Strategy 1.

also assume that the nuclear (U400) and hydro (U50) generators are must-run units [5]. The value of lost load or curtailing renewable generation is equal to $2000 per megawatt-hour. There are three wind farms each with the same power capacity, and they are installed at buses 16, 17 and 18. Wind data is taken from [16]. Here we ignore the uncertainty of loads and we assume that there are no storage assets present.

We run Strategies 1 and 3 from the previous subsection for comparison. Strategy 1 is as before, but here M is set to be 24 hours. Strategy 3 is the myopic policy to serve as the benchmark. Since temporal trends have already been discussed in last section, here we focus more specifically on the spatial correlation between the wind farms. For this, we introduce another energy scheduling strategy.

Strategy 4: This is also a flexibility-based energy scheduling strategy. However, under this Strategy the power outputs of wind farms are assumed to be independent. The scheduling framework, (7)–(24), is used as is, but Steps 2 and 5 are skipped when generating the spatial-temporal flexibility requirement envelopes.

In this section, a whole year of operation is considered. A unit commitment is executed at the beginning of each hour. The unit commitment is held fixed for each hour, and a receding horizon economic dispatch runs for every $T_\Delta = 5$ min.

Figure 9 displays the performance metrics for Strategies 1, 3 and 4 as we vary simultaneously the three wind farm capacities. As expected, Strategy 1 always has the lowest total generation cost. We can also find that the myopic strategy incurs much more load shedding and wind power curtailment. Comparing the results of Strategies 1 and 4, we find that ignoring the spatial correlation between wind farms leads to an increase (with an average of 3.5%) in total generation cost. At the same time, the differences in terms of ENS and EC between Strategy 1 and 4 are negligible.

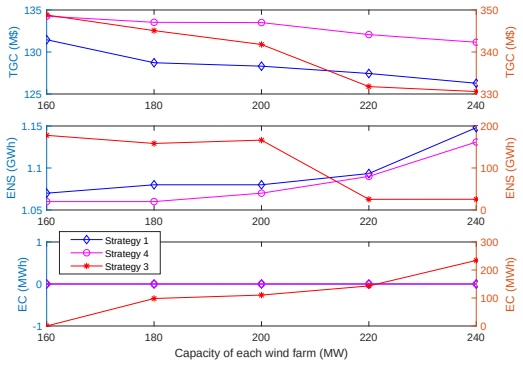

Figure 9: Performance metrics of Strategies 1, 4 and 3 in one year's operation with different wind farms capacities. The y-axis of Strategy 3 (in red) is on the right.

Scatter plots of the power output of three wind farms (when their respective capacities are of 240 MW) are shown in Figure 10(a) and (b); these clearly show their spatial correlation. In Figure 10(c) and (d), we project the 60-minute spatio-temporal flexibility requirement envelope generated by Strategy 1 and Strategy 4 onto two planes. For each strategy, the projection is made at 8:10 AM

on January 1st. By inspection of Figure 10, we find that Strategy 1 can effectively capture the spatial correlation between the three wind farms and reduce the size of the underlying flexibility requirement envelope. As a result, in Figure 11 we can see that the transmission line envelopes $\{e^{\uparrow}_{F_{18}}, e^{\downarrow}_{F_{18}}\}$ and $\{e^{\uparrow}_{F_{36}}, e^{\downarrow}_{F_{36}}\}$ generated by Strategy 1 are less conservative than those generated by Strategy 4. Though the flexibility requirement envelopes produced by Strategy 1 in Figure 11 are less conservative, it can be observed that the actual power flow trajectories remain inside respective envelopes.

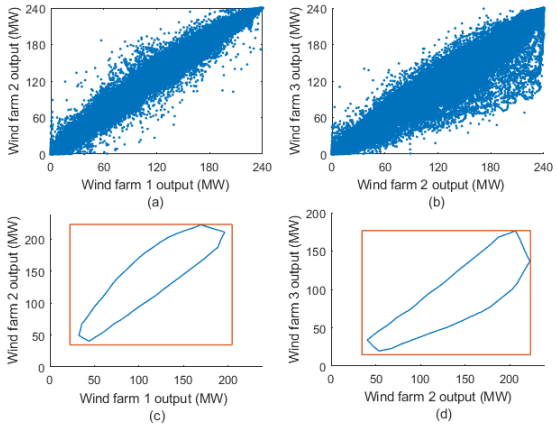

Figure 10: (a) and (b) are scatter plots of power outputs of three wind farms. (c) and (d) Projections of the spatio-temporal flexibility requirement envelopes in the wind farm 1-wind farm 2 and the wind farm 2 -wind farm 3 plane. The blue enclosures are generated by Strategy 1, and the red ones are generated by Strategy 4.

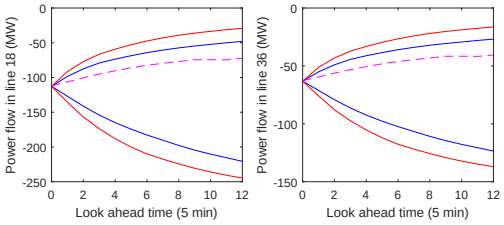

Figure 11: Transmission line capacity envelopes: (a) $\{e^{\uparrow}_{F_{18}}, e^{\downarrow}_{F_{18}}\}$ and (b) $\{e^{\uparrow}_{F_{36}}, e^{\downarrow}_{F_{36}}\}$. Blue lines are generated by Strategy 1, red lines are generated by Strategy 4. The dashed lines in magenta are actual trajectories.

Figure 12 shows the power flow in lines 18 and 36 and the unit commitment solutions produced by Strategy 1 and Strategy 4 on January 1st when all the three wind farms have the capacity of 240 MW. Strategy 4 tends to commit more generators and results in less cost-effective operation. This is because the larger flexibility requirement envelopes produced by Strategy 4 make it overestimate the potential risk of flow violations in transmission lines. Also in Figure 12, the power flow in line 18 and line 36 under Strategy 4 is always lower than that under Strategy 1 (negative represents the direction of power flow). Thus, the available transmission line capacities are not as fully exploited by Strategy 4 than under Strategy 1.

Finally, Figure 13 shows the performance of the three energy scheduling strategies when network constraint are ignored. By inspection of Figure 9 and Figure 13, we see that the three strategies will perform better when we only consider the power balancing constraint. As expected, Strategy 3 still behaves the worst, while Strategies 1 and 4 have similar performances. The difference between the results with the network seen between Strategies 1 and 4 reinforces the value of adequately treating spatial correlation; that value is much lower when ample transmission capacity is available as seen in Figure 13.

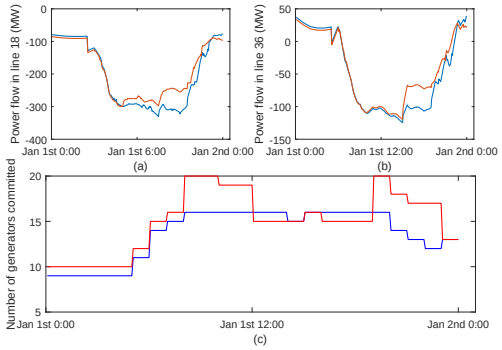

Figure 12: Power flow in (a) line 18 and (b) line 36 on Jan 1st. (c) is the number of generators committed by Strategy 1 and 4 on Jan. 1st. Blue lines are generated by Strategy 1, red lines are generated by Strategy 4.

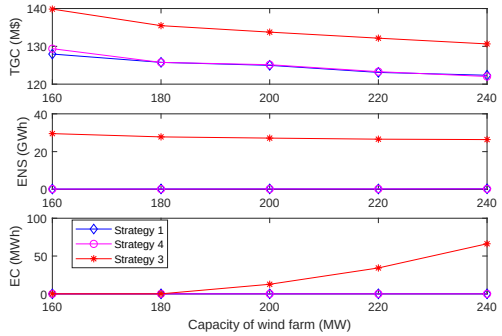

Figure 13: Performance metrics of Strategies 1, 4 and 3 in one year's operation with different wind farms capacities neglecting the transmission network.

5 Conclusion

In this paper, we proposed spatio-temporal flexibility requirement envelopes for managing flexibility and scheduling energy in power systems with significant variable renewable generation. Using historic generation and demand data, it can comprehensively capture and model the temporal trends and spatial correlation of multisite renewable generation and load demand. A mathematical program is also developed for applying the proposed variability modeling approach into power system energy scheduling through projections of the spatio-temporal envelopes. We conducted case studies to showcase the effectiveness of our approach both in microgrid context and in a larger transmission system. Results show that spatio-temporal flexibility requirement envelopes can effectively capture the temporal trends and spatial correlation of input power profiles by eliminating unlikely-to-happen scenarios, which effectively reduces the over-conservatism of the resulting envelopes. We observed that, as a result, the flexibility of storage in a microgrid and the full capacity of transmission lines in a transmission system can be better exploited. This leads to a decrease in total energy scheduling cost over the year but without incurring more load shedding or renewable generation curtailment compared with other flexibility scheduling methods. Key open questions remain in terms of better capturing longer-term renewable generation variabilities (e.g., seasonality) and in developing online envelope updating approaches.

Appendix A Gaussianization and PCA

Time series $\omega'_n(t)$ and $\delta^{s\prime}_n(t)$ are transformed into corresponding Gaussian time series by [13], [14]:

$$y''_n(t) = \Phi^{-1}\left[\hat{F}^y_n\left(y'_n(t)\right)\right] \tag{28}$$

where $y'_n(t)$ is equal to $\omega'_n(t)$ for wind speed/load time series or $\delta^{s\prime}_n(t)$ for solar power time series at bus n. $\hat{F}^y_n$ is the estimated cumulative distribution function (CDF) of $y'_n(t)$, while $\Phi(\cdot)$ is the CDF of the standard normal distribution.

The Gaussianized time series are assembled into the matrix $\mathbf{Y}''$, whose rows are $y''_n(t)$ and $\mathbf{\Sigma}$ is its covariance matrix. Letting $\lambda_1 \geq \lambda_2 \geq \cdots \geq \lambda_J$ be the eigenvalues of $\mathbf{\Sigma}$ and their corresponding eigenvectors $U_1, U_2, \cdots, U_J$, the matrix containing all J principal components (PC) of $\mathbf{Y}''$ is [14]:

$$\mathbf{Z}=[U_1\ U_2\ \cdots\ U_J]^T\mathbf{Y}'' \tag{29}$$

The jth ($1 \leq j \leq J$) row of $\mathbf{Z}$ is the jth PC of $\mathbf{Y}''$, where we note that J is equal to the number of separate location-specific time series. All the PC of $\mathbf{Y}''$ are uncorrelated and normally-distributed. Therefore, they are independent of each other [14], [18]. Moreover, as the PC index j increases, the relevance of the components decreases in capturing the variability of the time series (as seen with the decreasing values of the corresponding λ_j). The PCA transformation in (29) can be inverted back through:

$$\mathbf{Y}'' = [U_1\ U_2\ \cdots\ U_J]\mathbf{Z} \tag{30}$$

Appendix B Parameters of diesel generators and storage

From [19], we take for the diesel generators: $g^{c\max} = 500$ kW, $g^{c\min} = 30$ kW, $r^{csu} = 100$ kW/5 min, $r^{csd} = 500$ kW/5 min, $r^{cup} = r^{cdn} = 100$ kW/5 min, $a = 1.52 \times 10^{-5}$ l/kW^{2}h, $b = 0.02186$ l/kWh and $c = 41.6$ l/h. Cost of diesel fuel = \$1.30/l. For the storage: $g^{o\max} = 100$ kW, $g^{o\min} = -100$ kW, $s^{o\max} = 90$ kWh, $s^{o\min} = 10$ kWh, $\eta^c = \eta^d = 0.963$, $\pi^d = \pi^\delta = 100$ \$/kWh.

References

[1] International Energy Agency, Harnessing Variable Renewables: A Guide to the Balancing Challenge, Paris, France: IEA, 2011.

[2] H. Nosair and F. Bouffard, Flexibility envelopes for power system operational planning, IEEE Trans. Sustain. Energy, 6(3):800–809, July 2015.

[3] M. A. Bucher, S. Chatzivasileiadis and G. Andersson, Managing flexibility in multi-area power systems, IEEE Trans. Power Syst., 31(2):1218–1226, March 2016.

[4] F. Bouffard, F. D. Galiana and A. J. Conejo, Market-clearing with stochastic security-part I: formulation, IEEE Trans. Power Syst., 20(4):1818–1826, Nov. 2005.

[5] F. Bouffard, F. D. Galiana and A. J. Conejo, Market-clearing with stochastic security-part II: case studies, IEEE Trans. Power Syst., 20(4):1827–1835, Nov. 2005.

[6] H. Nosair and F. Bouffard, Economic dispatch under uncertainty: the probabilistic envelopes approach, IEEE Trans. Power Syst., 32(3):1701–1710, May 2017.

[7] C. Shao, X. Wang, M. Shahidehpour, X. Wang and B. Wang, Security-constrained unit commitment with flexible uncertainty set for variable wind power, IEEE Trans. Sustain. Energy, 8(3):1237–1246, July 2017.

[8] Y. Dvorkin, M. Lubin, S. Backhaus and M. Chertkov, Uncertainty sets for wind power generation, IEEE Trans. Power Syst., 31(4):3326–3327, July 2016.

[9] H Nosair and F. Bouffard, Energy-Centric Flexibility Management in Power Systems, IEEE Trans. Power Syst., 31(6):5071–5081, Nov. 2016.

[10] X. Jiang, Y. C. Chen and A. D. Dominguez-Garcia, A set-theoretic framework to assess the impact of variable generation on the power flow, IEEE Trans. Power Syst., 28(2):855–867, May 2013.

[11] P. Li, X. Guan, J. Wu and X. Zhou, Modeling dynamic spatial correlations of geographically distributed wind farms and constructing ellipsoidal uncertainty sets for optimization-based generation scheduling, IEEE Trans. Sustain. Energy, 6(4):1594–1605, Oct. 2015.

[12] Y. Guan and J. Wang, Uncertainty sets for robust unit commitment, IEEE Trans. Power Syst., 29(3):1439–1440, May 2014.

[13] J. Ekström, M. Koivisto, I. Mellin, R. J. Millar and M. Lehtonen, A Statistical Model for Hourly Large-Scale Wind and Photovoltaic Generation in New Locations, in IEEE Trans. Sustain. Energy, 8(4):1383–1393, Oct. 2017.

[14] D. D. Le, G. Gross and A. Berizzi, Probabilistic modeling of multisite wind farm production for scenario-based applications, IEEE Trans. Sustain. Energy, 6(3):748–758, July 2015.

[15] J. Heckenbergerova, P. Musilek and J. Marek, Analysis of wind speed and power time series preceding wind ramp events, in Proc. 2014 Int. Scientific Conf. on Electric Power Engineering, Brno, 2014, pp. 279–283.

[16] National Renewable Energy Laboratory. (2017). Renewable Resource Data [Online]. Available: https://www.nrel.gov/grid/renewable-resource-data.html.

[17] R. D. Zimmerman, C. E. Murillo-Sanchez and R. J. Thomas, MATPOWER: steady-state operations, planning, and analysis tools for power systems research and education, IEEE Trans. Power Syst., 26(1):12–19, Feb. 2011.

[18] B. Klockl, Multivariate time series models applied to the assessment of energy storage in power systems, in Proc. 10th Int. Conf. Probablistic Methods Applied to Power Systems, Rincon, 2008, pp. 1–8.

[19] M. Ross, C. Abbey, F. Bouffard and G. Joós, Multiobjective optimization dispatch for microgrids with a high penetration of renewable generation, IEEE Trans. Sustain. Energy, 6(4):1306–1314, Oct. 2015.